J Mater Sci (2009) 44:3072–3076
DOI 10.1007/s10853-009-3407-x

The role of friction to the indentation size effect in amorphous and crystallized Pd-based alloy

Ning Li · L. Liu · M. Zhang

Received: 11 December 2008 / Accepted: 16 March 2009 / Published online: 8 April 2009

Abstract The role of friction between the indenter and the test specimen in amorphous and crystallized $Pd_{40}Cu_{30}Ni_{10}P_{20}$ alloy was investigated through instrumented nanoindentation under unlubricated and lubricated conditions. It was found that the reduction of hardness with the increasing penetration depth, i.e., the indentation size effect (*ISE*), becomes milder in the lubricated test than that in the unlubricated measurement. The important role of friction that related to the surface area to volume (*S*/*V*) was discussed in terms of the proportional specimen resistance (*PSR*) model and energy dissipation.

Introduction

Instrumented nanoindentation techniques have been extensively used for the micromechanical characterization of materials due to their high time and spatial resolution [1, 2]. During nanoindentation, the hardness is often found to decrease with increasing indentation depth, i.e., the so called indentation size effect (*ISE*) [3]. Since the discovery of the *ISE* in crystalline materials, many mechanisms have been offered for its explanation, such as the strain gradient effects [4–6], the role of friction between the indenter facets and the test specimen [7, 8], surface effect [9], structural non-uniformity of the deformed volume [10], mixed elastic and plastic deformation response of material [11], etc. The variety of proposed mechanisms emphasizes the rather complicated nature of the *ISE*. However, most of the mechanisms developed are based on the dislocations theory for crystalline materials. In large indentations, the statistically stored dislocations (*SSDs*) can easily accommodate the shear stress. On the contrary, the geometrically necessary dislocations (*GNDs*) have to be created in order to form the residual indentations at small indentation depths, in which the density of geometrically necessary dislocations (*GNDs*) that is proportional to the strain gradient becomes appreciable [12].

In spite of the lack of dislocations in metallic glasses, the indentation size effect has also been reported recently in metallic glasses. In early work concentrating specifically on metallic glasses, Wright et al. [13] attributed the *ISE* to a reduction in shear band density with decreased peak load. Recently, the strain-induced softening due to the introduction of excessive free volume during plastic deformation [14–16], has been proposed as a main mechanism for the ISE [17, 18], while other authors have attempted to consider more complex hypotheses such as strain gradient hardening [19]. However, the detailed mechanism for the *ISE* has not been clearly understood. The contribution of friction between the indenter facets and the test specimen is expected more significant in nanoindentation [7]. More recently, Li et al. [20] suggests that, this friction effects may be sufficiently explanatory for the *ISE*, but an exact description of the role of friction during nanoindentation is a challenge, and to the best of our knowledge, the related experiment has not yet been studied. In this work, the *ISE* was investigated in amorphous and crystallized $Pd_{40}Cu_{30}Ni_{10}P_{20}$ alloy under unlubricated and lubricated conditions.

N. Li (✉) · L. Liu · M. Zhang
State Key Lab for Materials Processing and Die and Mould Technology, Huazhong University of Science and Technology, Wuhan 430074, People's Republic of China
e-mail: hslining@gmail.com

L. Liu
e-mail: lliu2000@mail.hust.edu.cn

M. Zhang
e-mail: flowoer@gmail.com

It is shown that the lubrication weakens the indentation size effect.

Experimental process

The amorphous $Pd_{40}Cu_{30}Ni_{10}P_{20}$ cylindrical rod with a diameter of 12 mm was prepared by water quenching of the alloy melt in a sealed quartz tube. The crystallized sample was prepared by annealing the amorphous alloy at 423 °C for 4 h in vacuum. The structure of the as-cast and of the annealed samples was examined by X-ray diffraction (*XRD*, Philips χ' Pert PRO) and differential scanning calorimetry (*DSC*, Perkin–Elmer DSC-7).

Nanoindentation experiments were carried out using a Triboindenter instrumented nanoindenter (from Hysitron, Minneapolis, MN) with a Berkovich diamond indenter, calibrated with pure aluminum and silica. In all the experiments, the temperature and air humidity inside the apparatus chamber were kept constant. Prior to nanoindentation, the surfaces of the samples were carefully polished to a mirror finish. The indentations were performed under load control at a loading rate of 0.5 mN s^{-1}. Lubricated measurements were made with a very thin layer of polybutene applied to the polished specimen surface. In order to obtain different indentation depths, samples were loaded under different maximum loads (P_{max}) ranging from 2 to 10 mN. At least six indents were made at each load to verify the accuracy and scatter of the indentation data.

Results

Figure 1 shows the *XRD* patterns obtained from the as-cast and annealed $Pd_{40}Cu_{30}Ni_{10}P_{20}$ alloy. Evidently, the as-cast alloy is of amorphous structure characterized by only a broad diffraction hump in its *XRD* pattern, while the annealed one is fully crystallized as indicated by a series of diffraction peaks indexed as Ni_2Pd_2P and $P_{3.2}Pd_{12}$ intermetallic compounds.

Figure 2 shows the typical load–depth (*P–h*) curves for the amorphous and crystallized $Pd_{40}Cu_{30}Ni_{10}P_{20}$ alloy, respectively, obtained under applied load of 10 mN at a loading rate of 0.5 mN s^{-1}. It is noted that the *P–h* curves show strong structure dependence. In the amorphous alloy which is free of dislocations, the *P–h* curve is punctuated by a number of discrete bursts of pop-ins. In contrast, the crystallized one exhibits a relatively smooth *P–h* curve under the same experimental condition. In addition, similar *P–h* curves are observed under unlubricated and lubricated measurements between the two alloys, indicating the identical deformation behavior.

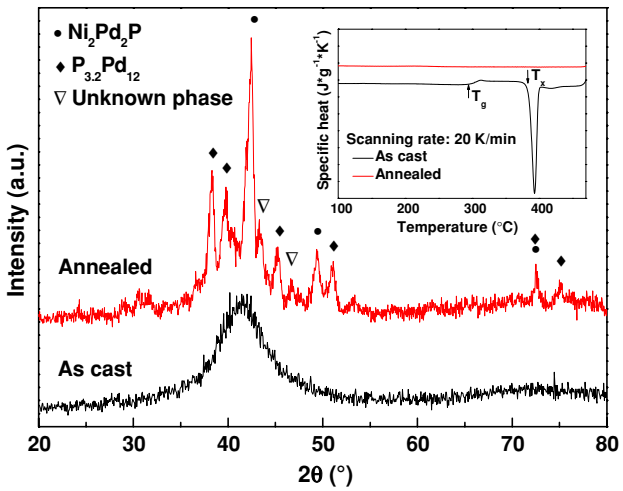

Fig. 1 XRD patterns of amorphous and crystallized $Pd_{40}Cu_{30}Ni_{10}P_{20}$ alloy [21]

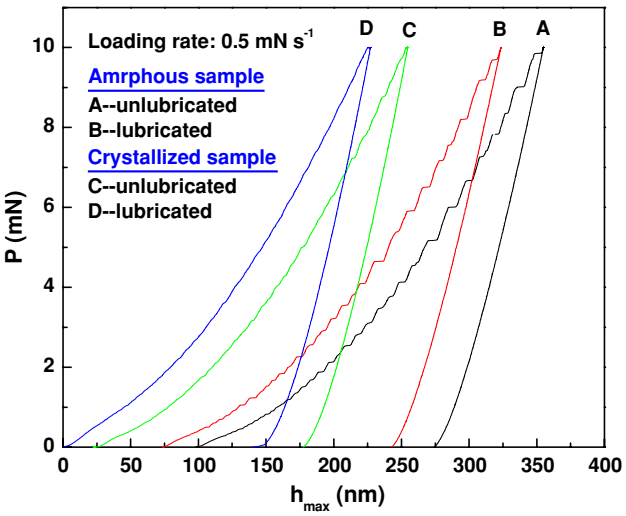

Fig. 2 Load–depth (*P–h*) of amorphous and crystallized $Pd_{40}Cu_{30}Ni_{10}P_{20}$ alloy in different (unlubricated or lubricated) measurements

Figure 3 shows the variation of the nanoindentation hardness (*H*) as a function of the maximum penetration depths (h_{max}) in the amorphous and crystallized $Pd_{40}Cu_{30}Ni_{10}P_{20}$ alloy, where *H* is calculated from Oliver–Pharr approach [22]. It can be seen clearly that the indentation hardness in both amorphous and crystallized $Pd_{40}Cu_{30}Ni_{10}P_{20}$ alloys, more or less decrease with the increase of the penetration depth, demonstrating the so called "indentation size effect (ISE)". However, different hardness reduction also can be observed under unlubricated and lubricated measurements. Obviously, the lubrication weakens the hardness reduction with increasing indentation depth, indicating an important role of the friction to the indentation size effect.

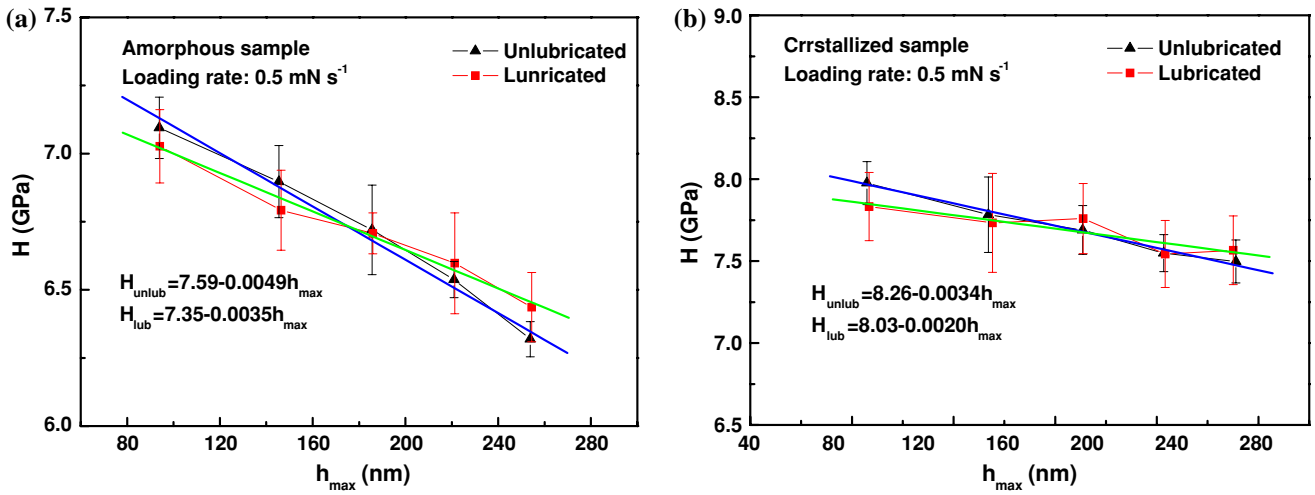

Fig. 3 Effect of lubrication on the hardness with different indentation depths in amorphous (**a**) and crystallized (**b**) $Pd_{40}Cu_{30}Ni_{10}P_{20}$ alloy

Discussion

The above experimental results clearly indicate that the friction contributes to the indentation size effect both in amorphous and crystallized $Pd_{40}Cu_{30}Ni_{10}P_{20}$ alloy. During nanoindentation, when an indenter is impressed into the test specimen surface, the local contact stress is very high at the contact surface between the indenter and the specimen. However, this high stress will be reduced if the frictional force parallel to the indenter facet/specimen interface, this effect will increase as the indentation size decreases because the indentation conditions involve a higher indentation surface (S) to deformation volume (V) ratio (S/V) [23]. By examining S/V, Li et al. [7] demonstrated the important contribution of friction to the Vickers microhardness of iron. For Berkovich indenter used in present study, $S/V = 1.79/h_c$, (h_c is the contact indentation depth), from which one can find that the ratio S/V dramatically decreases as the indentation becomes deeper, indicating that the contribution of friction to the indentation size effect is not constant but increases as the indentation size becomes smaller at lower indentation size [24].

The frictional contribution to the indentation size effect has been analyzed through a proportional specimen resistance (PSR) model that is proposed by Li et al. [23]. According to the model, indentation hardness can be described as being made up of two different parts: the indentation load-dependent part and the indentation load-independent part, as expressed by:

$$P_{\max} = a_1 h_c + a_2 h_c^2 \quad (1)$$

where $P_{\max}$ is the maximum indentation test load, a_1 is the coefficient describing the proportional specimen resistance, a_2 is the coefficient that is related to the load-independent micro-hardness, i.e., the so called "True hardness; H_{PSR}". Equation 1 can also be rearranged as:

$$P_{\max}/h_c = a_1 + a_2 h_c \quad (2)$$

Applying the data obtained in the present work to Eq. 2, the plots of $P_{\max}/h_c$ against h_c for both amorphous and crystallized alloy under unlubricated and lubricated conditions are obtained, as shown in Fig. 4a and b. From which the best fit a_1 and a_2 parameters can easily be calculated from the intersection point and slope of the curve, respectively, as described in Table 1, in which a notable difference of a_1 under unlubricated and lubricated tests can be clearly observed in the two alloys. For instance, the values of a_1 are around 16.24 and 16.72 uN/nm, respectively, under unlubricated measurement; however, the values of a_1 are substantially reduced by the lubrication, and drop to 15.36 and 15.86 uN/nm for the two alloys under lubricated test, demonstrating a significant friction role to the indentation size effect.

Multiply h_c in both sides, Eq. 1 also can be reformed as:

$$P_{\max} \cdot h_c = a_1 h_c^2 + a_2 h_c^3 \quad (3)$$

where $P_{\max} \cdot h_c$ is the total work (E_T) calculated from the area under the loading curve; For the $a_1 h_c^2$, Sangwal [25] and Fröhlich et al. [26] regarded it as the energy dissipated in new surface area creation, and Li et al. [7, 23], on the other hand, referred it to the energy dissipated ($E_{friction}$) due to the friction at the indenter facets/specimen interface and elastic resistance, here $E_{friction}$ can be calculated from the area enclosed in an indentation loading–unloading curve. As to $a_2 h_c^3$, which can be understood by the energy dissipated for the permanent deformation or volume creation

during nanoindentation. According to the above analysis, the values of $E_{friction}$, E_T can be calculated from the load–depth (P–h) curves, and the ratio $E_{friction}/E_T$ is plotted as a function of the maximum indentation depth (h_{max}), as depicted in Fig. 5a and b. It is found that the value of $E_{friction}/E_T$ decreases with the increasing indentation depth,

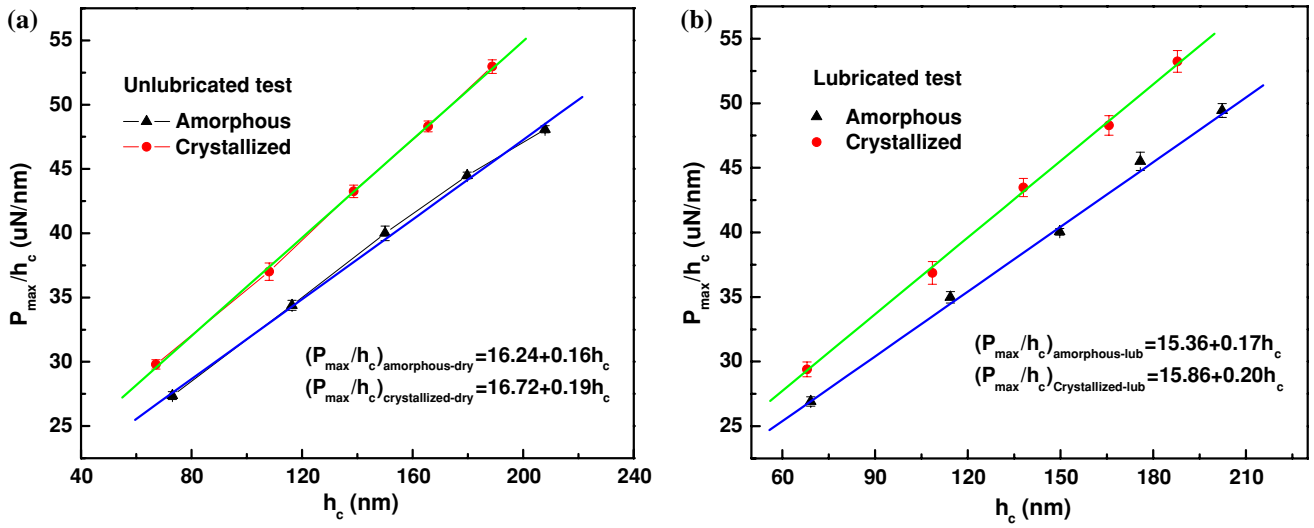

Fig. 4 The PSR model applied for the amorphous and crystallized $Pd_{40}Cu_{30}Ni_{10}P_{20}$ alloy under unlubricated (**a**) and lubricated (**b**) measurements

Table 1 Best fit parameters and analysis results according to the PSR model

Sample	Test conditions	a_1 (uN/nm)	a_2 (uN/nm^2)	Correlation factor (R^2)
Amorphous	Unlubricated	16.244	0.155	0.9991
	Lubricated	15.361	0.167	0.9986
Crystallized	Unlubricated	16.723	0.191	0.9997
	Lubricated	15.867	0.197	0.9995

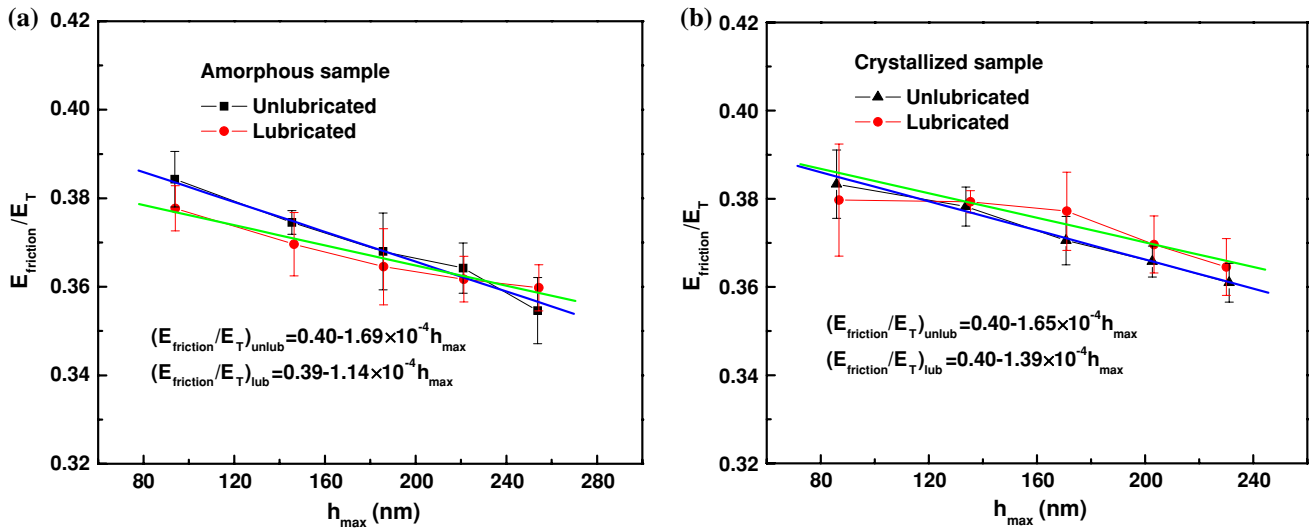

Fig. 5 Dependence of energy dissipation ratio ($E_{friction}/E_T$) on the indentation depths for the amorphous (**a**) and crystallized (**b**) $Pd_{40}Cu_{30}Ni_{10}P_{20}$ alloy under unlubricated and lubricated measurements

indicating that the friction is a function of the indentation depth. However, the reduction of $E_{friction}/E_T$ with the increasing indentation depth, more or less, becomes milder under lubricated measurement than that under unlubricated test; which is attributed to the lubrication that decreases the frictional energy dissipation, demonstrating the important role of friction to the indentation size effect.

Conclusions

In summary, the role of friction between the indenter and the test specimen in amorphous and crystallized $Pd_{40}Cu_{30}Ni_{10}P_{20}$ alloy was investigated through instrumented nanoindentation under unlubricated and lubricated conditions. The hardness reduction with the increasing penetration depth becomes milder in the lubricated test than that in the unlubricated measurement, which is attributed to the role of friction between indenter and the test specimen, and illustrated from the PSR model and energy dissipation point.

Acknowledgements This work was financially supported by the National Nature Science Foundation of China under Grant No. 50635020. The work was also partially supported by the funding from the Department of Industrial System and Engineering, the Hong Kong Polytechnic University. The authors are grateful to the Analytical and Testing Center, Huazhong University of Science and Technology for their technical assistance.

References

1. Schuh CA, Nieh TG (2004) J Mater Res 19:46
2. Schuh CA (2006) Mater Today 9:32
3. Joshi SS, Melkote SN (2004) J Manuf Sci Eng 126:679
4. Nix WD, Gao H (1998) J Mech Phys Solids 46:411
5. Gao H, Huang Y, Nix WD (1999) Naturwissenschaften 86:507
6. Gao H, Huang Y, Nix WD et al (1999) J Mech Phys Solids 47:1239
7. Li H, Ghosh A, Han YH et al (1993) J Mater Res 8:1028
8. Atkinson M (1995) J Mater Res 10:2908
9. Gerberich WW, Tymiak NI, Grunlan JC et al (2002) J Appl Mech 69:433
10. Skinner J, Gane N (1972) J Phys D: Appl Phys 5:2087
11. Bull SJ, Page TF, Yoffe EH et al (1989) Philos Mag Lett 59:281
12. Wei YG, Wang XZ, Zhao MH (2004) J Mater Res 19:208
13. Wright WJ, Saha R, Nix WD (2001) Mater Trans 42:642
14. Spaepen F (1977) Acta Metall 25:407
15. Concustell A, Sort J, Alcalá G et al (2005) J Mater Res 20:2719
16. Bei H, Xie S, George EP (2006) Phys Rev Lett 96:105503
17. Van Steenberge N, Sort J, Concustell A et al (2007) Scr Mater 56:605
18. Yang FQ, Geng KB, Law PK et al (2007) Acta Mater 55:321
19. Lam DCC, Chong ACM (2001) Mater Sci Eng A 318:313
20. Li N, Chan KC, Liu L (2008) J Phys D: Appl Phys 41:155415
21. Li N, Liu L, Chan KC et al (2009) J Mater Res (online)
22. Oliver WC, Pharr GM (1992) J Mater Res 7:1564
23. Li H, Bradt RC (1993) J Mater Sci 28:917. doi:10.1007/BF00400874
24. Shi H, Atkinson M (1990) J Mater Sci 25:2111. doi:10.1007/BF01045774
25. Sangwal K, Surowsk B, Błaziak P (2002) Mater Chem Phys 77:511
26. Fröhlich F, Grau P, Grellmann W (1977) Phys Stat Sol 42:79